



Excitation Spectra and luminescence decay analysis of K+ compensated Dy³⁺ doped CaMoO₄ phosphors

Journal:	<i>RSC Advances</i>
Manuscript ID:	RA-ART-10-2014-012447.R2
Article Type:	Paper
Date Submitted by the Author:	16-Dec-2014
Complete List of Authors:	Dutta, Somrita; Indian School of Mines, Applied Physics Som, Sudipta; Indian School of Mines, Applied Physics Sharma, Shailendra; Indian School of Mines, Department of Applied Physics

ARTICLE

Excitation Spectra and luminescence decay analysis of K^+ compensated Dy^{3+} doped $CaMoO_4$ phosphors

S Dutta, S Som and S K Sharma*

Department of Applied Physics, Indian School of Mines, Dhanbad 826004, India

Telephone: +913262235412

Fax: +913262296563

*Corresponding author E Mail: sksharma.ism@gmail.com

A series of Dy^{3+}/K^+ doped calcium molybdate phosphors were synthesized by hydrothermal synthesis method and the structural, photoluminescence and decay studies were carried out. Crystal structure and phase of the prepared phosphors were investigated using X-ray diffraction (XRD), Transmission electron microscopy (TEM) and Fourier transform infrared spectroscopy (FTIR). These studies show that the phosphors are of tetragonal structure with nanorod morphology. The photoluminescence results indicate that these phosphors could be efficiently excited by the near-ultraviolet radiation which causes the emission in the blue and yellow regions. A novel approach was used to calculate different spectral parameters of powder samples using excitation spectra instead of conventional absorption spectra. Quantitative calculation of spectral parameters, luminescence decay and quantum yield suggest the suitability of this phosphor as efficient luminescent media for light emitting devices.

1. Introduction

Study of optical spectra of rare-earth (RE) ions doped phosphors has been an active area of research due to their wide application in solid-state lasers, lighting and display devices^{1,2}. As an effective laser/ luminescent media Calcium Molybdate, $CaMoO_4$ is a promising host candidate for properties such as high melting point (1445–1480°C), high refractive index (1.98), average decay time (14 ms), quantum yield (9%), absorption cross section ($\sim 10^3 \text{ cm}^{-1}$)³. Therefore, luminescence properties of different rare earth doped $CaMoO_4$ phosphor have been studied previously to achieve a good luminescent media⁴⁻⁷.

The performance of luminescent materials can be assessed by the knowledge of Judd–Ofelt (JO) intensity parameters Ω_t ($t = 2, 4, 6$), spontaneous emission probabilities, oscillator strength and radiative branching ratios. The Ω_2 parameter is associated with the polarization and asymmetry of the RE ligands. The other two parameters $\Omega_{4,6}$ depend on long range effects. However, it is very difficult to calculate the JO intensity parameters for powder materials since the quantitative absorption spectra of powder materials can hardly be measured especially for the case of low RE dopant concentration. Now a days, with the development of novel nanophosphors for various display and lighting applications, it is very much required to find more convenient methods for the

determination of JO intensity parameters in case of powder materials, which are essential to predict RE spectral properties for a variety of material applications. An approach simply based on the measurement of the excitation spectra has been proposed by W Luo et al. to determine the JO parameters for RE^{3+} ions doped powders⁸. The approach has been successfully applied to three systems: NGW:Er, YLF:Nd and $Y_2O_3:Er^{3+}$ nanocrystals and the obtained JO parameters using this approach were in good agreement with that determined from the conventional method.

As per our literature survey till date no work has been reported on the estimation of JO parameters of doped /codoped $CaMoO_4$ phosphors. The authors have already reported the luminescence properties of this K^+ compensated Dy^{3+} doped $CaMoO_4$ phosphors⁹. Keeping this in view, an attempt was made for the first time to estimate different spectral parameters, luminescence decay time and quantum yield of the optimized Dy^{3+} doped and K^+ compensated codoped phosphor from the excitation spectra.

2. Experimental

2.1. Sample synthesis

Doped $Ca_{1-x}MoO_4: Dy_x^{3+}$ ($x = 0, 0.01, 0.015, 0.02, 0.03, 0.04, 0.05$) phosphors and codoped $Ca_{1-x-y}MoO_4: Dy_x^{3+}K_y^+$ ($x = 0.02, y = 0.01,$

0.02, 0.03, 0.04, 0.05) phosphors were prepared by hydrothermal synthesis. The reactants CaCO_3 , $(\text{NH}_4)_6\text{Mo}_7\text{O}_{24}\cdot 4\text{H}_2\text{O}$, Dy_2O_3 and K_2CO_3 were weighted in an appropriate stoichiometric ratio. All reagents were analytical grade and used without further purification. In a typical synthesis, solution A was prepared by dissolving CaCO_3 and Dy_2O_3 in diluted nitric acid. The solution was heated to drive away the unreacted nitric acid, and the residue was redissolved in 10 mL of deionized water and stirred for about 1 hour at room temperature. $(\text{NH}_4)_6\text{Mo}_7\text{O}_{24}\cdot 4\text{H}_2\text{O}$ was dissolved in 50 mL of deionized water named solution B. After stirring for about 15 minutes, solution B was added dropwise into the solution A under vigorous stirring. The pH of the solution was adjusted in between 8-9 using NaOH solution (1N). The resulting precursor solution was further stirred for about half an hour. After that, the solution was poured into 80-mL capacity Teflon-lined stainless steel autoclave and further heated to 180°C for 12 hours. After cooling down to room temperature naturally, the nanophosphors were directly collected at the bottom of the vessel. The phosphors were filtered, washed several times with deionized water and absolute ethanol, and dried in oven at 100 °C for 5 hours¹⁰. For the preparation of codoped phosphors, solution A was prepared by dissolving CaCO_3 , Dy_2O_3 and K_2CO_3 in diluted nitric acid and rest of the procedure was same.

2.2. Sample characterization

X-Ray diffractogram of the prepared phosphors were recorded in a wide range of Bragg angle 2θ ($10^\circ \leq 2\theta \leq 80^\circ$) using Bruker D8 X-Ray diffractometer with CuK_α radiation ($\lambda = 0.154056$ nm). FTIR studies were carried out on Perkin Elmer make Spectrum RX1 Spectrometer. Morphology and crystallite size of the phosphors were determined by JEOL make JEM-2100 transmission electron Microscope. Photoluminescence studies were carried out on Hitachi make F-2500 Fluorescence Spectrophotometer in the wavelength range 220 nm - 700 nm. The decay kinetics was studied on Quanta Master 40 fluorometer. All the studies were carried out at room temperature.

2.3. THEORETICAL BACKGROUND

2.3.1. Judd–Ofelt theory

The J-O theory^{11,12} has been extensively used to analyze the radiative transitions of rare-earth ions in several host materials. The electric-dipole (ED) and magnetic-dipole (MD) transitions are mainly used to calculate the line strengths of optical spectra of RE^{3+} ions in luminescent materials. For most of the transitions, the probability for magnetic dipole transitions is much smaller than those for the forced electric dipole transitions [$A_{\text{md}}[J \rightarrow J'] < A_{\text{ed}}[J \rightarrow J']$]. However, in certain cases, they may significantly contribute to the total $J \rightarrow J'$ radiative transition probability.

The excitation line strength for an ED transition can be expressed in terms of J-O intensity parameters $\Omega_2, \Omega_4, \Omega_6$ by

$$S_{\text{calc}}^{\text{ed}}(J \rightarrow J') = \sum_{t=2,4,6} \Omega_t \left| \langle \varphi J \| U^{(t)} \| \varphi' J' \rangle \right|^2 \quad (1)$$

where the matrix elements $\langle \varphi J \| U^{(t)} \| \varphi' J' \rangle$ are doubly reduced unit tensor operator¹³ of rank t calculated in the intermediate coupling approximation and are independent of the crystal host. The parameters Ω_2, Ω_4 , and Ω_6 exhibit the influence of the host on the transition probabilities since they contain the crystal-field parameters, inter configurational radial integrals, and the interaction between the central ion and intermediate environment. The reduced matrix elements of the unit tensor $\langle \varphi J \| U^{(t)} \| \varphi' J' \rangle$ were taken from ref. 14.

The measured line strengths ($S_{\text{meas}}^{\text{ed}}$) were calculated from the excitation spectrum by:

$$S_{\text{meas}}^{\text{ed}}(J \rightarrow J') = \frac{3ch(2J+1)}{8\pi^3 \lambda e^2 N_0} \frac{9n}{(n^2+2)^2} \Gamma_{\text{exc}} \quad (2)$$

where J (J') is the angular momentum quantum number of the initial (final) state of rare earth ion, n is the refractive index of the sample, λ is the mean wavelength of the excitation band, N_0 is rare earth ion concentration and Γ_{exc} is the integrated excitation intensity for each band from the initial state to the final state which is similar to the integrated absorbance for the absorption spectrum⁸. The factor $[9n/(n^2+2)]^2$ in Eq. 2 is the local field correction for the ion in the dielectric host medium. The measured line strengths were then used to obtain the J-O parameters Ω_2, Ω_4 , and Ω_6 by solving a set of n number of equations for the corresponding transitions between J and J' . A least squares fit method was used for Eqns. (1) and (2) to get a good fit between the calculated and measured line strengths as well as to obtain J-O intensity parameters (Ω_t).

The magnetic-dipole transitions are parity allowed between states of the $4f^N$ configuration and are subject to the selection rules, $\Delta l=0$, $\Delta S=0$, $\Delta L=0$, $|\Delta J| \leq 1$, (but not $0 \leftrightarrow 0$) in the Russel – Saunders limit¹⁵. The line strengths due to the magnetic dipole contribution were determined using the following expression:

$$S_{\text{calc}}^{\text{md}}(J \rightarrow J') = \left(\frac{eh}{4\pi mc} \right)^2 \left| \langle (SLJ) \| L + 2S \| (S'L'J') \rangle \right|^2 \quad (3)$$

The line strengths of the bands due to magnetic dipole transition are determined from the corresponding values of oscillator strengths, $f_{\text{calc}}^{\text{md}}$ using the following expression:

$$S_{\text{calc}}^{\text{md}}(J \rightarrow J') = \frac{3h(2J+1)n^2}{8\pi^2 m c v} f_{\text{calc}}^{\text{md}} \quad (4)$$

Values of $f_{\text{calc}}^{\text{md}}$ were taken from Carnall et al¹⁶.

2.3.2. Radiative properties

The J–O parameters were used to predict the radiative properties of

the excited states of Dy^{3+} ion. The radiative transition probability (A_R) for a transition $J \rightarrow J'$ is calculated from the following equation¹⁷:

$$A_R(J \rightarrow J') = \frac{64\pi^4\nu^3}{3h(2J+1)} \left[\frac{n(n^2+2)^2}{9} S_{ed} + n^3 S_{md} \right] \quad (5)$$

where S_{ed} and S_{md} are the electric and magnetic-dipole line-strengths. The radiative lifetime (τ_R) of an excited state is given by

$$\tau_R(J) = \frac{1}{\sum_{J'} A_R(J \rightarrow J')} \quad (6)$$

The branching ratio (β_R) corresponding to the emission from an excited level J to lower level J' is given by

$$\beta_R(J, J') = \frac{A_R(J \rightarrow J')}{\sum_{J'} A_R(J \rightarrow J')} \quad (7)$$

The stimulated emission cross-section ($\sigma(\lambda_p)$) can be expressed as:

$$\sigma(\lambda_p)(J \rightarrow J') = \frac{\lambda_p^4}{8\pi c n^2 \Delta\lambda_{eff}} A_R(J \rightarrow J') \quad (8)$$

where λ_p is the peak wavelength and $\Delta\lambda_{eff}$ is its effective linewidth found by dividing the area of the emission band by its maximum height.

3. Results and Discussions

3.1. Structural analysis

3.1.1. XRD studies:

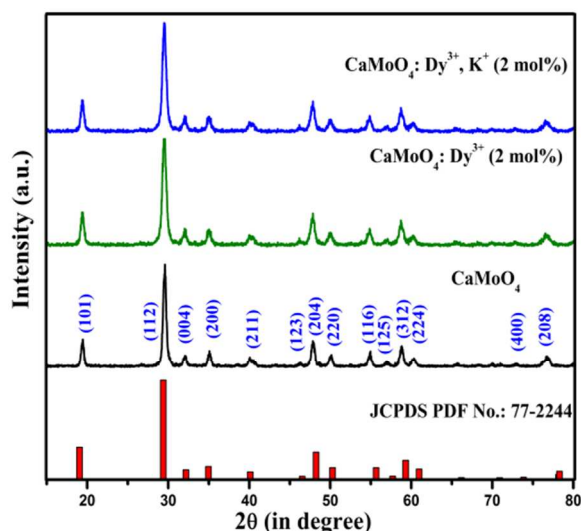


Figure 1. XRD spectra of CaMoO_4 phosphors.

Figure 1. shows the XRD spectra of undoped CaMoO_4 , 2 mol% Dy^{3+} doped CaMoO_4 and 2 mol % K^+ codoped CaMoO_4 phosphors. A single tetragonal phase was observed and diffraction peaks match with *JCPDS* card no 77-2244 with space group $I4_1/a$ (88).

The substitution of Dy^{3+} and K^+ for Ca^{2+} did not influence the phase and crystal structure of CaMoO_4 suggesting that dopant and codopant might have occupied the cationic sites in the host lattice structure, following the charge balancing¹⁸: $2\text{Ca}^{2+} = \text{Dy}^{3+} + \text{K}^+$. The enhancement of XRD peak intensities in codoped phosphor is due to the incorporation of K^+ thus improving the crystallinity. The (h k l) values of most prominent peaks are shown in the XRD pattern.

3.1.2 Rietveld refinement:

A structural refinement by the Rietveld method¹⁹ was performed using the Fullprof Program²⁰. Figure 2a. shows the Rietveld plot for undoped CaMoO_4 . The structural refinement results are presented in Table 1. Figure 2b. shows the schematic representation of the tetragonal CaMoO_4 unit cell. The unit cell was modelled through a program called Visualization for Electronic and Structural Analysis (VESTA)²¹ using Rietveld refinement data. The Ca and Mo sites have S_4 point symmetry. Its crystal structure has two building blocks of CaO_8 clusters with scalenohedral configuration and snub disphenoid polyhedra (8 vertices, 12 faces, and 18 edges) and MoO_4 tetrahedra. Due to the O-Mo-O bond angles, the $[\text{MoO}_4]$ clusters are slightly distorted into the matrix²². Each O atom links with two Ca atoms and one Mo atom. There are two different Ca-O bond lengths in CaO_8 and one Mo-O bond length in MoO_4 .

Table 1: Structural parameters of undoped CaMoO_4 after Rietveld refinement.

Atoms	Wyckoff	x	y	Z	Occupancy	Lattice consta
Ca	4b	0	0.25	0.625	0.250	a = b = 5.12
Mo	4a	0	0.25	0.125	0.250	c = 11.11
O	16a	0.090	0.398	0.306	1.000	

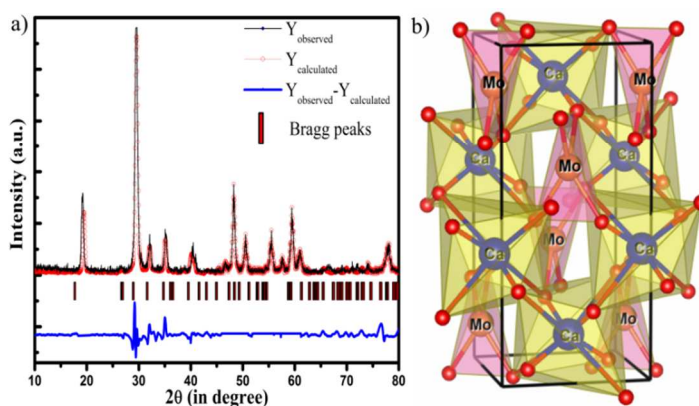


Figure 2. Rietveld refinement pattern and CaMoO_4 unit cell.

3.1.3. TEM Studies

TEM images of undoped CaMoO_4 phosphor is shown in Figure 3a. Nanorod like structures of 20 nm diameter was observed. The high resolution TEM (HRTEM) image suggests that phosphor is crystalline (Figure 3b). Its selected area electron diffraction (SAED) is shown in

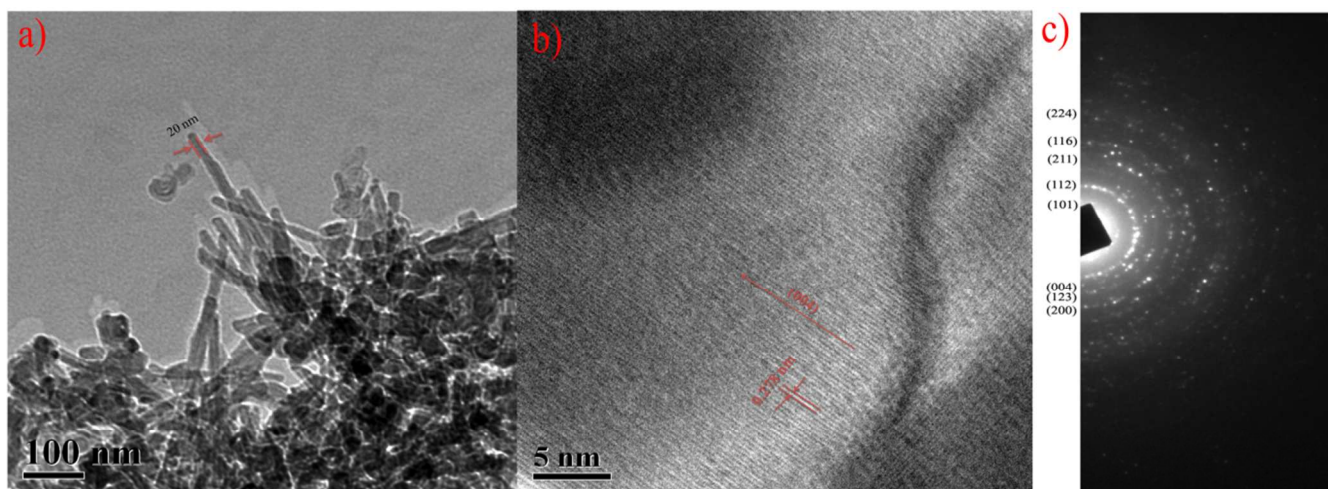


Figure 3. TEM studies of CaMoO_4 phosphor

Figure 3c. Based on a tetragonal phase, the rings are observed and (hkl) planes are indexed. The SAED pattern show the (101), (112), (004), (200), (123), (211), (116) and (224) planes in good agreement with the XRD result. The lattice fringe was observed and $d = 2.78 \text{ \AA}$, which matches with $hkl = 004$ plane of tetragonal phase.

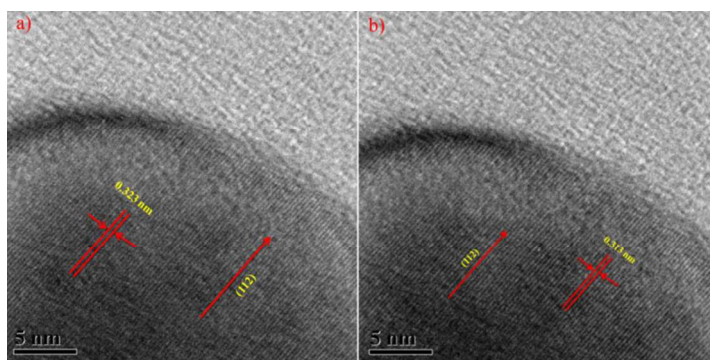


Figure 4. HRTEM studies of a) doped b) codoped CaMoO_4 phosphors.

Figure 4a and b show the HRTEM images of Dy^{3+} (2 mol %) doped and Dy^{3+} , K^+ (2 mol %) codoped phosphors. It clearly shows an improvement in crystallinity and $d = 3.23 \text{ \AA}$ for doped and $d = 3.13 \text{ \AA}$ for codoped phosphor, which matches with $hkl = 112$ plane.

3.1.4. FTIR Studies

FTIR spectra of the undoped, Dy^{3+} (2 mol %) doped, K^+ (2 mol %) codoped phosphors in wave number range of $4000\text{--}400 \text{ cm}^{-1}$ are shown in Figure 5. It can be seen that all the phosphors show approximately similar vibrations. The strong absorption band occurring at 805 cm^{-1} is due to the asymmetric stretching vibrations in the $[\text{MoO}_4]^{2-}$ clusters and a weak band at 432 cm^{-1} is due to the presence of asymmetric bending vibrations present in the O-Mo-O bonds.¹⁸ The inset illustrates a characteristic $[\text{MoO}_4]$ cluster with asymmetric stretching and asymmetric bending vibrations between

the O-Mo-O bonds. The bands at 1652 and 3419 cm^{-1} correspond to H-O-H bending and O-H stretching vibrations of water molecules present on the surface of particles respectively. The 1383 cm^{-1} vibration is due to the N-O band of HNO_3 used during the preparation of sample. The peaks observed at 2382 and 2925 cm^{-1} in the as-prepared sample indicates C-H stretching vibration.²³

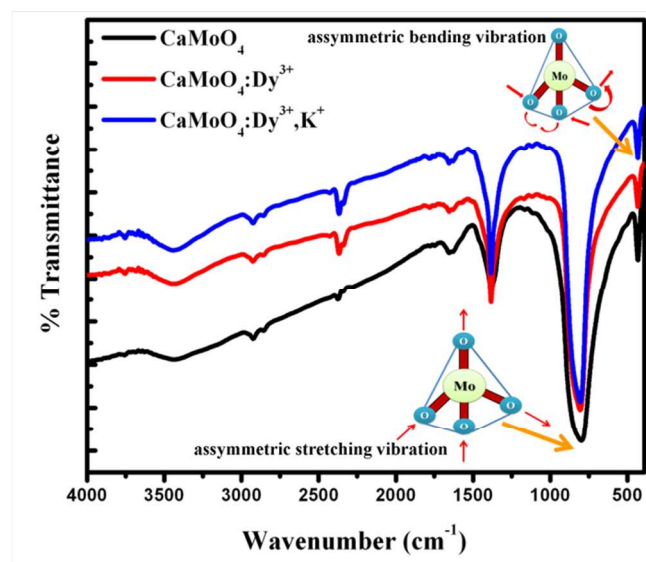


Figure 5. FTIR of CaMoO_4 phosphors.

3.2. Luminescence analysis

3.2.1. Excitation Spectra

The excitation spectra of Dy^{3+} doped CaMoO_4 with different Dy^{3+} ion concentrations (1, 1.5, 2, 3, 4 and 5 mol %) and K^+ codoped CaMoO_4 : Dy^{3+} with varying concentration of K^+ (1, 2, 3, 4, 5 mol %) and optimum Dy^{3+} concentration at 2 mol % are shown in Figure 6a. The spectra exhibit a broad band from 220 nm to 330 nm with a maximum centred at 275 nm . This is due to charge transfer from oxygen (O^{2-}) to metal (Mo^{6+}) ion.²⁴ The other peaks²⁵ at 351 nm (${}^6\text{H}_{15/2} \rightarrow {}^6\text{P}_{7/2}$), 366 nm (${}^6\text{H}_{15/2} \rightarrow {}^4\text{M}_{19/2} + {}^4\text{D}_{3/2} + {}^6\text{P}_{5/2}$), 387 nm (${}^6\text{H}_{15/2} \rightarrow {}^4\text{M}_{21/2} + {}^4\text{K}_{17/2} + {}^4\text{F}_{7/2} + {}^4\text{I}_{13/2}$), 427 nm (${}^6\text{H}_{15/2} \rightarrow {}^4\text{G}_{11/2}$), 452 nm (${}^6\text{H}_{15/2} \rightarrow {}^4\text{I}_{15/2}$) and 475 nm (${}^6\text{H}_{15/2} \rightarrow {}^4\text{F}_{9/2}$) are due to f-f transition of

Dy³⁺. These transitions are magnified in Figure 6b.

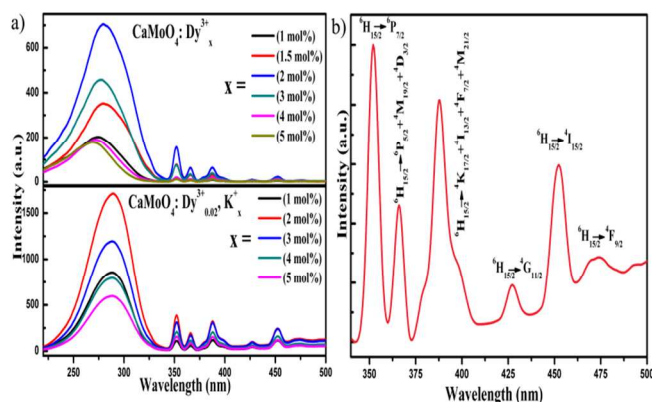


Figure 6. Excitation spectra of CaMoO₄ phosphors.

3.2.2. J – O parameters

From the excitation spectra the measured line strengths (S_{meas}) were determined by using Eq. (1). The Judd - Ofelt parameters Ω_2 , Ω_4 , Ω_6 were obtained using least-squares fitting approach between the S_{meas} and the S_{cal} . The J – O parameters, for various Dy³⁺ concentrations and for 2 mol% K⁺ codoped CaMoO₄ phosphors are tabulated in Table 2 along with the previously reported value for CaMoO₄: Dy²⁶.

Table 2: Judd-Ofelt intensity parameters

Phosphor	Mol %	Ω_2 $\times 10^{-20}$ (cm ²)	Ω_4 $\times 10^{-20}$ (cm ²)	Ω_6 $\times 10^{-20}$ (cm ²)	rms ΔS $\times 10^{-20}$ (cm ²)
CaMoO ₄ :Dy ³⁺ _x	x = 1	50.34	2.71	9.78	0.577
	x = 1.5	9.58	1.89	4.78	0.033
	x = 2	7.21	1.41	3.59	0.052
	x = 3	7.88	0.96	2.92	0.024
	x = 4	21.30	0.89	3.33	0.036
	x = 5	17.41	0.58	2.89	0.024
CaMoO ₄ :Dy ³⁺ _x ,K ⁺ _y	x = 2, y = 2	40.94	1.36	6.18	0.406
CaMoO ₄ :Dy (from literature)	1 wt %	0.266	2.89	1.79	

There is not much variation of Ω_4 and Ω_6 with change in the Dy³⁺ concentration. But the experimental value of Ω_2 is most sensitive to the ligand environment which can be clearly observed by the change of its value with concentration of Dy³⁺ and also with incorporation of K⁺ ions. Higher value of Ω_2 indicates high degree of metal-ligand covalency bond and lower symmetry of the coordination structure surrounding the Dy³⁺ ions²⁷. The high Ω_2 value indicates the possession of high charge density for Dy³⁺ ion which polarizes the O²⁻ anion to a much greater extent. This result in a larger extent of molecular orbital overlap between the f orbital of the Dy³⁺ and the p orbital of the O²⁻ ion, resulting in expansion of the electron cloud and the formation of a bond having less ionic and more covalent character. The decrease in Ω_2 value decreases orbital overlap between Dy³⁺ and O²⁻ and hence the covalent character²⁸.

The root mean square (rms) deviation between the experimental and calculated line strengths is defined as:

$$rms\Delta S = \sqrt{\frac{\sum_{i=1}^N (S_{meas} - S_{cal})^2}{N - 3}} \quad (9)$$

where N is the number of experimental bands involved in the above calculation. The value of the rms ΔS reflects the goodness of the J-O parameters fitting.

3.2.3 Emission Spectra

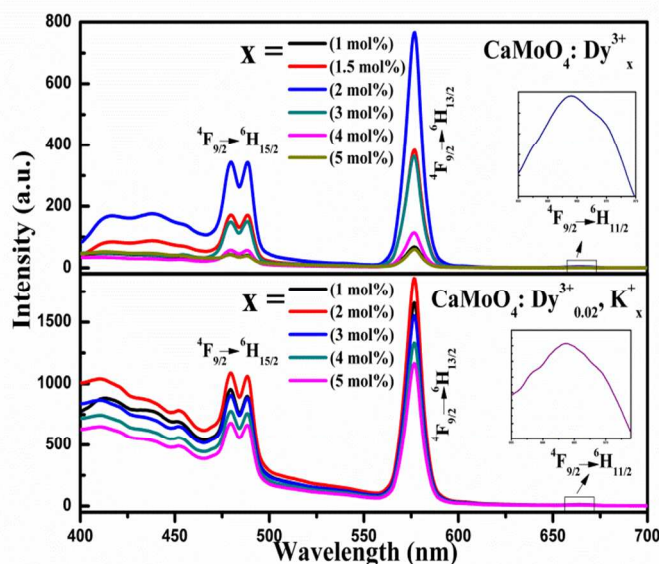


Figure 7. Emission spectra of doped and codoped CaMoO₄ phosphors.

Figure 7. represents the emission spectra of doped/codoped CaMoO₄ phosphors as a function of Dy³⁺ and K⁺ concentration. Three peaks observed at 489, 576 and 663 nm is assigned to ⁴F_{9/2}→⁶H_{15/2} (blue), ⁶H_{13/2} (yellow) and ⁶H_{11/2} (red) transitions, respectively. The transition ⁴F_{9/2}→⁶H_{11/2} is of very low intensity which is magnified in the inset. The ⁴F_{9/2}→⁶H_{13/2} transitions are hypersensitive electronic dipole transitions with $\Delta J = 2$, which are greatly affected by the coordination environment and are allowed only at low symmetries with no inversion centre. In this case, the dominance of this transition indicates that the location of Dy³⁺ deviates from the inversion symmetry, i.e., at low symmetry positions. This also corroborates the fact that Ω_2 has a high value which implies the asymmetric coordination surrounding Dy³⁺ ions^{18, 29}.

The luminescence intensity increases with increase of concentration of Dy³⁺ ions upto 2.0 mol % and then decreases. Quenching of luminescence with increasing Dy³⁺ ion concentration takes place as the distance between the neighboring Dy³⁺ ions decreases with the increase of Dy³⁺ ions. This decrease in the distance between the ions reduces the radiative transitions, thereby increasing the non-radiative energy transfer through cross relaxation channels. Keeping the Dy³⁺ concentration at 2 mol%, the

K^+ mol concentration was varied from 1 to 5 mol% where the maximum intensity was recorded at 2 mol% of K^+ . This was due to the charge compensation phenomena as $2Ca^{2+} = Dy^{3+} + K^+$. This K^+ codoping increases the nonradiative decay paths for excited Dy^{3+} which increases the emission intensity. But further increase in K^+ greater than 2 mol% increases the lattice distortion which reduces the emission intensity⁹.

From the calculated J–O intensity parameters, the spectral parameters such as radiative transition probability (A_R), life-time (τ_R) and branching ratio (β_R) were calculated. The emission spectra were used to calculate the parameters like peak emission wavelength (λ_p), effective line widths ($\Delta\lambda_{eff}$) and the peak emission cross-section ($\sigma(\lambda_p)$) using Eqs.(5) – (8). Experimental branching ratio (β_{exp}) was obtained by using the relative intensities of individual peaks to that of the total intensity of emission peaks. All the spectral parameters including A_T and τ_R for the excited ${}^4F_{9/2}$ level are tabulated in Table 3.

Table 3: Spectral parameters

Phosphor	Transition ${}^4F_{9/2} \rightarrow$	β_{exp}	β_{cal}	A_R $\times 10^3$ (sec^{-1})	$\sigma(\lambda_p)$ $\times 10^{-20}$ cm^2
CaMoO ₄ :Dy ³⁺ _{0.02}	${}^6H_{15/2}$	0.306	0.111	0.619	0.100
	${}^6H_{13/2}$	0.691	0.844	4.6996	1.52
	${}^6H_{11/2}$	0.031	0.045	0.2525	0.103
$A_T = 5.5711, \tau_R = 179.5 \mu s$					
CaMoO ₄ :Dy ³⁺ _{0.02} ,K ⁺ _{0.02}	${}^6H_{15/2}$	0.355	0.093	0.7865	0.079
	${}^6H_{13/2}$	0.631	1.015	8.6093	2.56
	${}^6H_{11/2}$	0.003	0.010	0.0869	0.029
$A_T = 8.4827, \tau_R = 105.5 \mu s$					

The radiative lifetimes of the ${}^4F_{9/2}$ level decreases from 179.5 μs to 105.5 μs with the incorporation of K^+ ions. From the emission spectra as well as from the values of β_{exp} , it was found that the ${}^4F_{9/2} \rightarrow {}^6H_{13/2}$ transition sweeps most of the intensity emitted by the phosphor. The radiative transition probability and peak emission cross-section were also found to be higher for ${}^4F_{9/2} \rightarrow {}^6H_{13/2}$ transition compared to the other transitions. This high $\sigma(\lambda_p)$ value suggests that the ${}^4F_{9/2} \rightarrow {}^6H_{13/2}$ transition has potential application for lasing action.

Further, in order to compare the luminescence intensity, the intensity area under the curve of magnetic and electric dipole transitions was determined by fitting with Gaussian distribution function

$$I = I_B + \sum_{i=1}^n \frac{A_i}{w_i \sqrt{\pi/2}} e^{-\frac{2(\lambda - \lambda_{ci})^2}{w_i^2}} \quad (10)$$

where I is intensity, I_B is the background intensity, w_i is the width at half maximum intensity of the curve, and A_i is area under the curve. λ is wavelength and λ_{ci} is the mean wavelength value corresponding to the transition. All the fittings were carried out in

the range of 450–510 and 535–615 nm for magnetic and electric dipole transitions, respectively. The relative intensity ratio ${}^4F_{9/2} \rightarrow {}^6H_{13/2}$ to ${}^4F_{9/2} \rightarrow {}^6H_{15/2}$ transitions can be used as sensitive parameter for understanding the symmetry around the Dy^{3+} in the host material. This parameter is called asymmetric ratio (A_{12})³⁰ and is defined as

$$A_{21} = \frac{\int_{510}^{615} I_2 d\lambda}{\int_{450}^{510} I_1 d\lambda} \quad (11)$$

where I_1 and I_2 represent the respective integrated intensities of ${}^4F_{9/2} \rightarrow {}^6H_{15/2}$ and ${}^4F_{9/2} \rightarrow {}^6H_{13/2}$ transitions of Dy^{3+} , respectively. This ratio varies from 2.22 to 2.25 with the variation of Dy^{3+} concentration. When K^+ is codoped the asymmetric ratio drastically decreases to 1.85. Higher value of A_{21} indicates more asymmetry around Dy^{3+} ligand. This indicates that with K^+ codoping the symmetry nature of Dy^{3+} ligand increases in the host matrix.

3.2.4. Quantum Yield

External quantum efficiency (EQE) generally known as quantum yield (η) is related to number of photons incident on the sample (α) and number of photons emitted (ϵ) as^{30,31}

$$\eta = \frac{\epsilon}{\alpha} = \frac{\int I_{emission}}{\int I_{solvent} - I_{sample}} \quad (12)$$

where $I_{emission}$ is luminescence emission spectrum of sample, $I_{solvent}$ is the spectrum of light used to excite only solvent and I_{sample} is the spectrum of light used for exciting sample. Quantum yields for 2 mol % Dy^{3+} doped and K^+ codoped phosphors found to be 5% and 8%, respectively.

3.2.5. Decay curve analysis

Theoretically, the measured lifetime (τ_{mes}) of the ${}^4F_{9/2}$ fluorescent level can be expressed as²⁰:

$$\frac{1}{\tau_{mes}} = \frac{1}{\tau_R} + W_{NR} \quad (13)$$

where τ_{mes} and τ_R are the measured and radiative lifetimes obtained from decay curves and J–O theory respectively. W_{NR} is the non-radiative relaxation rate which includes multi-phonon relaxation (W_{MP}), energy transfer through cross-relaxation (W_{CR}) and several other non radiative processes. The multi-phonon relaxation is inefficient owing to the significantly large energy gap between the ${}^4F_{9/2}$ emitting level and the next-lower level (about 8000 cm^{-1}) as compared with the maximum phonon energy of the matrix lattice²⁷. So only radiative transition and non-radiative energy transfer relaxation is responsible for the depopulation of the ${}^4F_{9/2}$ multiplet. The internal quantum efficiency (IQE) of the excited ${}^4F_{9/2}$ state (η) is given by equation

$$\eta = \frac{\tau_{mes}}{\tau_R} \quad (14)$$

This IQE is completely different from the EQE calculated before as explained in ref 32. Figure 8. shows the decay curves of Dy³⁺ ions at 576 nm emission of ⁴F_{9/2} excited level CaMoO₄ at 2 mol% concentration and 2 mol% K⁺ codoped CaMoO₄.

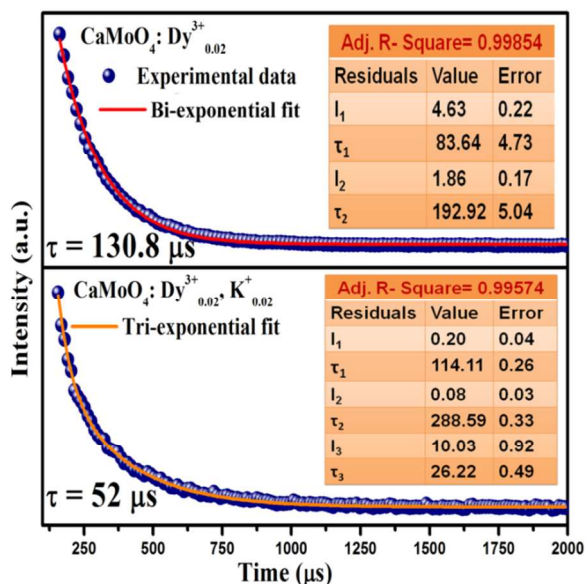


Figure 8. Luminescence decay curve of CaMoO₄ phosphors.

To understand behavior of luminescence decay, the decay data were fitted with different decay equations. It was found that curves follow two types of exponential decays for Dy³⁺ doped and Dy³⁺/K⁺ codoped phosphors respectively in the host viz, (i) bi-exponential decay

$$I(t) = I_1 e^{-\frac{t}{\tau_1}} + I_2 e^{-\frac{t}{\tau_2}} \quad (15)$$

where *I*₁ and *I*₂ are intensities at different times and their corresponding lifetimes *τ*₁ and *τ*₂.

The average lifetime in case of a bi-exponential decay can be calculated using the equation

$$\tau_{avg} = \frac{I_1 \tau_1^2 + I_2 \tau_2^2}{I_1 \tau_1 + I_2 \tau_2} \quad (16)$$

and (ii) triexponential decay

$$I(t) = I_1 e^{-\frac{t}{\tau_1}} + I_2 e^{-\frac{t}{\tau_2}} + I_3 e^{-\frac{t}{\tau_3}} \quad (17)$$

where *I*₁, *I*₂ and *I*₃ are intensities at different times and their corresponding lifetimes *τ*₁, *τ*₂ and *τ*₃.

The average lifetime in case of a tri-exponential decay can be calculated using the equation

$$\tau_{avg} = \frac{I_1 \tau_1^2 + I_2 \tau_2^2 + I_3 \tau_3^2}{I_1 \tau_1 + I_2 \tau_2 + I_3 \tau_3} \quad (18)$$

The multiexponential decay may be explained as²⁹:

(i) Difference in the nonradiative probability of decays for lanthanide ions at or near the surface and lanthanide ions in the core of the particles.

(ii) Inhomogeneous distribution of the doping ions in the host material leading to the variation in the local concentration.

(iii) The transfer of excitation energy from donor to lanthanide activators.

Moreover biexponential decay behavior has been reported for low concentration of lanthanide ions in different matrices which is also the case in the present paper.

The fluorescence lifetime *τ*_{meas} (*τ*_{avg}) of the ⁴F_{9/2} multiplet was calculated to be 130.80 μs for Dy³⁺ doped CaMoO₄ and decreases to 52 μs for K⁺ codoped CaMoO₄. The deviation between the *τ*_{meas} and *τ*_r (obtained from J-O theory) may be because the Judd–Ofelt theory is prone to overestimate the value of the radiative lifetime due to its partial inadequacy to predict the the radiative properties²⁷. Moreover, structural defects and the presence of several Dy³⁺ sites in the matrix may impact the ⁴F_{9/2} level emission, leading to *τ*_{meas} lower than expected. It is clearly seen from the result that after K⁺ codoping, the lifetime reduces. Codoping with K⁺ ion increases the nonradiative decay paths for excited Dy³⁺. This increases the nonradiative transition probability which increases the radiative luminescence emission rate³³. The increase in the total transition probability reduces the lifetime after K⁺ codoping as the lifetime is inverse of the total transition probability.

The IQE for the 2 mol% doped Dy³⁺ and 2 mol% K⁺ compensated CaMoO₄ phosphors were found to be 72.42% and 49.52% respectively.

4. Conclusion

The Judd–Ofelt theory, extended for powder phosphors using excitation spectra instead of conventional absorption spectra, has been successfully applied to evaluate the intensity parameters, radiative transition rates, branching ratios and radiative lifetimes relevant to the ⁴F_{9/2} level of Dy³⁺ ion in CaMoO₄ host. A strong yellow and blue emission bands were observed in the visible region upon efficient excitation by near UV light which was well matched with near UV LEDs. The phosphor was characterized by high values of emission cross-section and branching ratio for the ⁴F_{9/2} → ⁶H_{13/2} transition (yellow colour) which increases after K⁺ codoping. As reported previously, the doped/codoped CaMoO₄ phosphors can be utilized in commercial white LEDs and other display devices owing to its colour tunable property. In this present study the

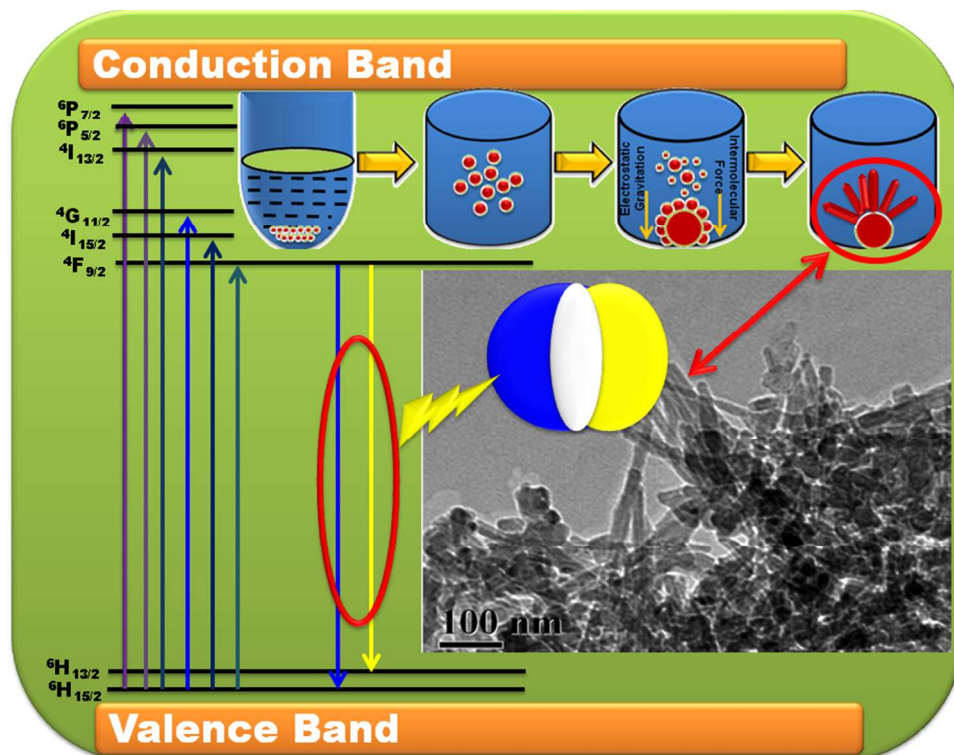
fluorescence and radiative lifetimes of $^4F_{9/2}$ level with suitable quantum efficiency also indicates that this doped / codoped phosphor may be efficiently used for solid-state yellow lasers pumped by commercially available blue laser diodes.

Acknowledgment

The authors are thankful to the Department of Science and Technology, New Delhi (Government of India) for funding this work under the Project SR/FTP/PS-087/2010. The authors are also thankful to Dr. R. Banerjee and Ms. Jonaki Mukherjee of CGCRI Kolkata for lifetime measurement.

References

1. Y. Tian, B. Chen, R. Hua, J. Sun, L. Cheng, H. Zhong, X. Li, J. Zhang, Y. Zheng, T. Yu, L. Huang and H. Yu, *J. Appl. Phys.*, 2011, **109**, 053511(1-6).
- 15 2. S.-P. Lee, C.-H. Huang, T.-S. Chan and T.-M. Chen, *ACS Appl. Mater. Interfaces*, 2014, **6**, 7260.
3. A. K. Parchur, R. S. Ningthoujam, S. B. Rai, G. S. Okram, R. A. Singh, M. Tyagi, S. C. Gadkari, R. Tewari and R. K. Vatsa, *Dalton Trans.*, 2011, **40**, 7595.
- 20 4. D. Gao, Y. Li, X. Lai, Y. Wei, J. Bi, Y. Li and M. Liu, *Mater. Chem. Phys.*, 2011, **126**, 391.
5. A. Xie, X. Yuan, S. Hai, J. Wang, F. Wang and L. Li, *J. Phys. D: Appl. Phys.*, 2009, **42**, 105107 (1-7).
6. Z. Hou, R. Chai, M. Zhang, C. Zhang, P. Chong, Z. Xu, G. and J. Lin, *Langmuir*, 2009, **25** (20), 12340.
7. S. Yan, J. Zhang, X. Zhang, S. Lu, X. Ren, Z. Nie and X. Wang, *J. Phys. Chem. C*, 2007, **111**, 13256.
8. W. Luo, J. Liao, R. Li and X. Chen, *Phys. Chem. Chem. Phys.*, 2010, **12**, 3276.
- 30 9. S. Dutta, S. Som and S. K. Sharma, *Dalton Trans.*, 2013, **42**, 9654.
10. Z. Chen, W. Bu, N. Zhang and J. Shi, *J. Phys. Chem. C*, 2008, **112**, 4378.
11. B. R. Judd, *Phys. Rev.*, 1962, **127**, 750.
- 35 12. G. S. Ofelt, *J. Chem. Phys.*, 1962, **37**, 511.
13. C. K. Jayasankar and E. Rukmini, *Opt. Mater.*, 1997, **8**, 193.
14. W. T. Carnall, H. Crosswhite and H. M. Crosswhite, *Argonne National Laboratory Report*, Argonne, IL, USA, 1978.
15. R. C. Powell, *Physics of Solid-State Laser Materials*. AIP, New York, 1998.
- 40 16. W. T. Carnall, P. R. Fields and K. J. Rajnak, *Chem. Phys.*, 1968, **49**, 4412.
17. V. Venkataramu, P. Babu, C. K. Jayasankar, Th. Tröster, W. Sievers and G. Wortmann, *Opt. Mater.*, 2007, **29**, 1429.
- 45 18. S. K. Sharma, S. Dutta, S. Som and P. S. Mandal, *J. Mater. Sci. Technol.*, 2013, **29**(7), 633.
19. H. M. Rietveld, *J. Appl. Crystallogr.*, 1969, **2**, 65.
20. J. Rodriguez -Carvajal, 2010, Full Comput. Program <http://www.ill.eu/sites/fullprof/php/downloads.html>
- 50 21. K. Momma and F. Izumi, *J. Appl. Crystallogr.*, 2008, **41**, 653.
22. V. S. Marques, L. S. Cavalcante, J. C. Sczancoski, A. F. P. Alcântara, M. O. Orlandi, E. Moraes, E. Longo, J. A. Varela, M. Siu Li and M. R. M. C. Santo, *Cryst. Growth Des.*, 2010, **10**, 4752.
- 55 23. A. K. Parchur and R. S. Ningthoujam, *Dalton Trans.*, 2011, **40**, 7590.
24. A. K. Parchur, A. I. Prasad, A. A. Ansari, S. B. Rai and R. S. Ningthoujam, *Dalton Trans.*, 2012, **41**, 11032.
25. J. S. Kumar, K. Pavani, A. M. Babu, N. K. Giri, S. B. Rai and L. R. Moorthy, *J. Lumin.*, 2010, **130**, 1916.
- 60 26. E. Cavalli, E. Bovero and A. Belletti, *J. Phys.: Condens. Matter*, 2002, **14**, 5221.
27. W. -W. Zhou, B. Wei, W. Zhao, G. -F. Wang, X. Bao, Y. -H. Chen, F. -W. Wang, J. -M. Du and H. -J. Yu, *Opt. Mater.*, 2011, **34**, 56.
- 65 28. T. Som and B. Karmakar, *J. Phys.: Condens. Matter*, 2010, **22**, 035603.
29. S. Som, A. K. Kunti, V. Kumar, V. Kumar, S. Dutta, M. Chowdhury, S. K. Sharma, J. J. Terblans and H. C. Swart, *J. Appl. Phys.*, 2014, **115**, 193101.
- 70 30. N. S. Singh, R. S. Ningthoujam, N. Yaiphaba, S. D. Singh and R. K. Vatsa, *J. Appl. Phys.*, 2009, **105**, 064303(1-7).
31. Y. K. Mishra, S. Kaps, A. Schuchardt, I. Paulowicz, X. Jin, D. Gedamu, S. Freitag, M. Claus, S. Wille, A. Kovalev, S. N. Gorb and R. Adelung, *Part. Part. Syst. Char.*, 2013, **30**, 775.
- 75 32. W. D. A. M. de Boer, C. McGonigle, T. Gregorkiewicz, Y. Fujiwara, S. Tanabe and P. Stallinga, *Scientific Reports*, 2014, **4**, 5235.
33. R. M. Bakker, V. P. Drachev, Z. Liu, H.-K. Yuan, R. H. Pedersen, A. Boltasseva, J. Chen, J. Irudayaraj, A. V. Kildishev and V. M. Shalaev, *New Journal of Physics*, 2008, **10**, 125022



Graphical abstract
254x190mm (96 x 96 DPI)